Estimating and Measuring Arterial Travel Time and Delay

Final Report

Prepared by:

Henry X. Liu
Xinkai Wu

Department of Civil Engineering
University of Minnesota

CTS 12-20

Technical Report Documentation Page

1. Report No.	2.	3. Recipients Accession No.	
CTS 12-20			
4. Title and Subtitle Estimating and Measuring Arterial Travel Time and Delay		5. Report Date August 2012 6.	
7. Author(s) Henry X. Liu and Xinkai Wu		8. Performing Organization Report No.	
9. Performing Organization Name and Address Department of Civil Engineering University of Minnesota 500 Pillsbury Drive, SE Minneapolis, MN 55455		10. Project/Task/Work Unit No. CTS Project #2010081 11. Contract (C) or Grant (G) No.	
12. Sponsoring Organization Name and Address Intelligent Transportation Systems Institute University of Minnesota 200 Transportation and Safety Building 511 Washington Ave. SE Minneapolis, Minnesota 55455		13. Type of Report and Period Covered Final Report 14. Sponsoring Agency Code	
15. Supplementary Notes http://www.its.umn.edu/Publications/ResearchReports/			

16. Abstract (Limit: 250 words)

To estimate arterial travel time/delay, the key element is to estimate intersection queue length, since travel time, delay, and level of services can be easily derived from queue length information. In this study, we developed a new traffic flow model, named shockwave profile model (SPM), to describe queuing dynamics for congested arterial networks. Taking advantage of the fact that traffic states within a congested link can be simplified as free-flow, saturated, and jammed conditions, the SPM simulates traffic dynamics by analytically deriving the trajectories of four major shockwaves. This model is particularly suitable for simulating congested traffic especially with queue spillover. In the SPM, a novel approach is proposed as part of the SPM, in which queue spillover is treated as either extending a red phase or creating new cycles. Since only the essential features, i.e. queue build-up and dissipation, are considered, the SPM significantly reduces the computational load and improves the numerical efficiency. We further validated the SPM using real-world traffic signal data collected from a major arterial in the Twin Cities. The results clearly demonstrate its effectiveness and accuracy. This model can be applied to estimate arterial travel time and delay and optimize signal timing in real time.

17. Document Analysis/Descriptors		18. Availability Statement	
Arterial highways, Travel time, Traffic signal control systems, Queuing, Shockwave profile model, Cell transmission model, Traffic models		No restrictions. Document available from: National Technical Information Services, Alexandria, Virginia 22312	
19. Security Class (this report) Unclassified	20. Security Class (this page) Unclassified	21. No. of Pages 46	22. Price

Estimating and Measuring Arterial Travel Time and Delay

Final Report

Prepared by:

Henry X. Liu
Xinkai Wu

Department of Civil Engineering
University of Minnesota

August 2012

Published by:

Intelligent Transportation Systems Institute
Center for Transportation Studies
University of Minnesota
200 Transportation and Safety Building
511 Washington Ave. S.E.
Minneapolis, MN 55455

Acknowledgments

The authors wish to acknowledge Mr. Steve Misgen of the Minnesota Department of Transportation, who collaborated with the research team on the field implementation of the SMART-SIGNAL System. The study was funded by the Intelligent Transportation Systems (ITS) Institute, a program of the University of Minnesota's Center for Transportation Studies (CTS). Additional financial support was provided by the United States Department of Transportation Research and Innovative Technologies Administration (RITA).

Table of Contents

List of Figures

List of Tables

Executive Summary

Estimating and measuring travel times on arterials are challenging tasks. Unlike freeway traffic flow, arterial traffic flow is interrupted by signalized intersections. Travel time on arterials depends not only on traffic volumes, link capacities, and speed limit, but also on signal timing and queue length at intersections. The SMART-SIGNAL (Systematic Monitoring of Arterial Road Traffic and SIGNAL) system, developed by the University of Minnesota, offers an easily implementable approach to collect and archive continuous and high-resolution traffic data on signalized arterials. The availability of time-stamped signal status and vehicle-detector actuation data essentially allows us to reconstruct the history of traffic signal events along the arterial street. Therefore, it provides us the capability of predicting travel times and delays for current departure times as well as those in the near future by tracing an imaginary vehicle (i.e., a virtual probe). Based upon the SMART-SIGNAL system, we recently developed a virtual probe model to estimate real-time arterial travel time. However, the accuracy of queue length estimation significantly impacts the estimated travel time provided by the virtual probe model, especially under oversaturation scenarios.

Since the key element for arterial travel time estimation is to estimate queue length accurately, we further developed a new traffic flow model, named shockwave profile model (SPM), to describe queuing dynamics for congested arterial networks. Taking advantage of the fact that traffic states within a congested link can be simplified as free-flow, saturated, and jammed conditions, the SPM simulates traffic dynamics by analytically deriving the trajectories of four major shockwaves: queuing, discharge, departure, and compression waves. Unlike conventional macroscopic models, in which space is often discretized into small cells for numerical solutions, the SPM treats each homogeneous road segment with constant capacity as a section; and the queuing dynamics within each section are described by tracing the shockwave fronts. The SPM is particularly suitable for simulating traffic flow on congested signalized arterials especially with queue spillover problems, where the steady-state periodic pattern of queue build-up and dissipation process can break down. Depending on when and where spillover occurs along a signalized arterial, a large number of queuing patterns are possible. Therefore it becomes difficult to directly apply the conventional approach to track shockwave fronts. To overcome this difficulty, a novel approach is proposed as part of the SPM, in which queue spillover is treated as either extending a red phase or creating new smaller cycles, so that the analytical solutions for tracing the shockwave fronts can be easily applied. Since only the essential features of arterial traffic flow, i.e. queue build-up and dissipation, are considered, the SPM significantly reduces the computational load and improves the numerical efficiency when it is applied for travel time estimation.

We further validated the SPM using real-world traffic signal data collected from a major arterial in the Twin Cities. The results clearly demonstrate the effectiveness and accuracy of the model. This model can be applied to estimate arterial travel time and delay in real time. This model can also contribute to signal optimization.

Chapter 1. Introduction

Travel time and delay are important measures for evaluating transportation network performance and also the most understood measures for helping road users make informed travel decisions. However, it is well-known that accurately estimating arterial travel time on signalized arterials is not an easy task because of the periodic disruption on traffic flow by signal lights. It becomes even more difficult when the signalized links are congested with long queues. So far to the best of our knowledge, no reliable method is readily available to estimate real-time arterial travel times and delays under congested conditions. Although there exist a number of regression methods (Turner et al., 1996; Frechette & Khan, 1998; Zhang, 1999) and heuristic approaches (Takaba et al., 1991; Cheu et al., 2001), they were mainly targeted to provide offline steady state assessments using low-resolution (5-minute or longer) traffic volume and signal timing data.

Recently, built upon the Systematic Monitoring of Arterial Road Traffic Signals (SMART-SIGNAL) system, Liu and Ma (2009) developed a virtual probe model to estimate real-time arterial travel time. At each time step, the maneuver decision (acceleration, deceleration or no-speed-change) of the virtual probe is determined by its own state and its surrounding traffic conditions. Surrounding traffic states include the status of the queue ahead of the virtual probe and the signal status. The proposed approach is data-intensive, which utilizes both vehicle-actuation and signal phase change data from existing traffic signal systems. The availability of time-stamped signal status and vehicle-detector actuation data essentially allows us to reconstruct the history of traffic signal events along the arterial street. Therefore, it provides us the capability of predicting travel times and delays for current departure times as well as those in the near future by tracing an imaginary vehicle (i.e., a virtual probe).

Although the virtual probe model is feasible for real-time arterial travel time estimation and short-term prediction, it requires a known time-dependent queue length profile for each intersection along the arterial. It is self-evident that the accuracy of travel time estimation depends significantly on how well we can estimate the queue length. Accurate queue length information becomes particularly important for travel time estimation under congested conditions.

The widely-accepted queue length estimation method, i.e., the input-output method, has an inherent drawback. It cannot handle congested situations with long queues (long queue is defined here as that the queue length is longer than distance from intersection stop-bar to advance detector), unless a link entrance detector is available, which is usually not the case. Liu et al. (2009) addressed the long queue estimation problem by examining the queue discharge process and the intersection shockwave characteristics. Since the queue estimation method described in Liu et al. (2009) does not depend on the measurement of traffic arrival volume to the intersection, it can estimate the queue length that is much longer than the distance from intersection stop-bar to the advance detector. We should note that the focus of Liu et al. (2009) is to estimate the length of the standing queue, i.e. the motionless stacked vehicles behind the stop line.

Other popular approaches for queue estimation usually reply on traffic flow theories. Over the last fifty years, following the seminal works of Lighthill & Whitham (1955) and Richards (1956), continuum traffic flow theories have been studied by many researchers. For a recent review of current continuum traffic flow models, we refer to Zhang (2001). Although LWR-type models have been criticized for their inability to account for the acceleration and deceleration process of traffic flow, it has been argued that simple continuum models are sufficient to describe traffic behaviors in signalized networks, because, as one author put it, "traffic flow dynamics are dominated by external events (red traffic lights) rather than by the inherent traffic flow dynamics" (Papageorgiou, 1998). Michalopoulos *et al.* (1980) derived an analytical solution for describing the evolution of the queue length on a signalized link, based on the continuum principle and method of characteristics.

When applying traffic flow models to queue estimation, we have to face the obstacles of numerical errors and computational inefficiency. For numerical reasons, the solutions to continuum traffic flow models usually involve the discretization of space and time to describe the spatio-temporal variations of traffic flow and density. The well-known cell transmission model (CTM), indicated by its very name, applies the finite difference method to simulate the evolution of traffic density in each cell, whose length is equal to the distance traveled by a free-flowing vehicle in one time interval (Daganzo, 1994, 1995). When the CTM is applied to model arterial flow, however, numerical errors often occur because it is not uncommon that a signalized link cannot be decomposed into an integer number of cells. Although this may not be a problem if the cell size is small, using small sizes increases the number of cells for an arterial link, thereby compromising the computational efficiency.

In this report, we propose a section-based approach to model arterial traffic flow dynamics, which is adopted in the virtual probe model for estimating travel time. Instead of using the usual differential approach, we integrate traffic over finite road sections. Therefore a signalized road section will no longer be decomposed into uniform cells; rather, each homogeneous road segment with constant capacity is treated as a section and the major shockwaves generated within a section or between two adjacent sections are traced explicitly. We call our approach the shockwave profile model (SPM). We should note that the concept of a "section-based" traffic flow model was initially proposed by Helbing (2003), but it was applied to study freeway traffic flow for travel time analysis.

The purpose of the SPM is to provide a quick and approximate approach, with sufficient descriptive power, to model traffic flow dynamics in a signalized network for real-time travel time estimation. As indicated in Dell'Olmo and Mirchandani (1996), for real-time applications, signal control strategies need to be evaluated quickly. Therefore, it is not necessary to track traffic densities in each small cell; rather, it is important to track the tail of an intersection queue, because it directly impacts the travel of virtual probe when estimating travel time. Due to traffic lights, repetitive shockwaves for queue build-up and dissipation clearly separate a road section into three different traffic states: free-flow, saturated, and jammed. The proposed model takes advantage of these simplified traffic states to describe traffic dynamics. Such simplification allows us to derive an analytical solution for queuing dynamics, while reducing computational costs significantly.

The SPM applies the basic concept of the shock-fitting method, where shockwaves need to be assumed explicitly. The shock-fitting method has been criticized in previous research because of its complexity (Michalopoulos et al., 1984), while the shock-capturing approach has been popularly applied in many macroscopic traffic flow models including the CTM. Indeed, there are difficulties when applying the shock-fitting method to congested signalized arterials where cyclic stop-and-go traffic create many shockwaves and explicitly determining each wave becomes impossible. However, these difficulties have been solved in the SPM by reasonably simplifying traffic into four major waves which capture the essential traffic dynamics in congested arterials. Such simplification makes the SPM applicable and even attractive because it inherits the comparative advantages on computational accuracy and efficiency from the shock-fitting method (Michalopoulos et al., 1984).

Additionally, the SPM is particularly suitable for estimating travel time on congested signalized arterials especially with queue spillover problems, where the steady-state periodic pattern of queue build-up and dissipation process may break down. Depending on when and where the spillover happens along a signalized arterial, a large number of queuing patterns may be possible. Therefore the conventional approach to keep tracking shockwave fronts becomes much more complicated. To overcome the difficulty, a novel approach is proposed as part of the SPM, in which queue spillover is treated as either extending a red phase or creating new smaller cycles, so that the analytical solution for tracing shockwave fronts can be easily applied.

We also empirically validated the SPM, using the real-world traffic signal data collected by the SMART-SIGNAL system which was implemented on six consecutive intersections of Trunk Highway 55 in the Twin Cities (Liu and Ma, 2009; Liu et al., 2009). We compared the estimation results from the SPM against the field data for a PM peak during which a nine-cycle queue spillover occurred (Wu, et al., 2010). The results clearly demonstrate the effectiveness and accuracy of the proposed travel time estimation method.

The rest of report is organized as follows. Chapter 2 briefly reviews the SMART-SIGNAL system and the virtual probe model as the background for travel time estimation in this research. In Chapter 3, we introduce the SPM model for a signalized approach with or without downstream spillover. A discussion on the issues of model implementation follows in Chapter 4. In Chapter 5, we present a simple numerical example that demonstrates the difference between the CTM and the SPM in dealing with congested arterial traffic. Field validation results are given in Chapter 6. Finally, Chapter 7 concludes this report with some remarks.

Chapter 2. Background

The SMART-SIGNAL (Systematic Monitoring of Arterial Road Traffic and SIGNAL) system, developed by the University of Minnesota, offers an easily implementable approach to collect and archive continuous and high-resolution traffic data on signalized arterials (Liu *et al.*, 2008). In this system, a complete history of traffic signal control, including all vehicle actuation events and signal phase change events, is archived and stored. Based on the event-based data, arterial performance measures, such as arterial travel time, intersection queue length, and level of service, are produced. The SMART-SIGNAL system has been installed on 11 intersections along France Avenue in Hennepin County, Minnesota, and 6 intersections along Trunk Highway 55, Minnesota, since February 2007. Event-based traffic data are being collected in a 24/7 mode and then archived in a database system, thus yielding a tremendous amount of field data available for research. This chapter will briefly introduce the system architecture, data collection hardware, and data processing procedure of the SMART-SIGNAL.

2.1 SMART-SIGNAL System Architecture

As illustrated in Figure 2.1, the SMART-SIGNAL system has three major components, data collection, performance measurements, and performance presentation through user interfaces. The data collection component collects high resolution raw data directly from the field on an event-by-event basis. Signal phase change events and vehicle-detector actuation events are acquired separately from data collection units located in traffic signal cabinets. The event-based raw data will be packaged and sent to the data server located at the Minnesota Transportation Observatory (MTO) lab at the University of Minnesota through the Digital Subscriber Line (DSL) or wireless communication in real time. The second component of the SMART-SIGNAL system is performance measure calculation using the field-collected data. Analysis of the stored event data yields a set of performance measures, one covers intersection level measures (*e.g.* queue length) and a second related to arterial level measures (*e.g.* travel time). Once all performance measures have been derived from the raw data, the results are made accessible to a variety of users.

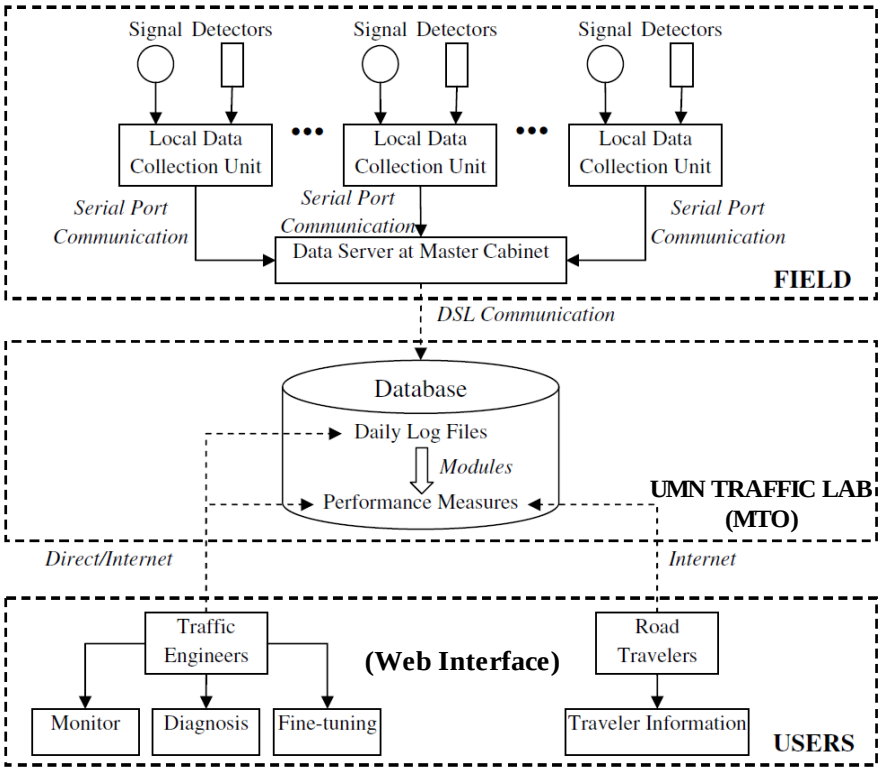

Figure 2.1 SMART-SIGNAL System Architecture (Source: Liu and Ma, 2009)

2.2 Data Collection Unit

The key element of the SMART-SIGNAL is the data collection unit, which consists of an industrial PC and a data acquisition card. At each intersection, an industrial PC with a data acquisition card is installed, and event data collected at each intersection is transmitted to the data server in the master controller cabinet through the existing communication line (in this case, spare twisted pair) between signalized intersections. The data acquisition cards (PCI-6511 from National Instruments (2006)) used in the SMART-SIGNAL system, as shown in Figure 2.2a, have 64 input channels. If the total number of detector inputs and signal phases for one intersection exceed 64, an additional data acquisition card needs to be installed. A terminal box is used in order to limit the input direct current (DC) to a safe range and establish the connection between the data acquisition card and back panel of the traffic cabinet, as shown in Figure 2.2b. The terminal box allows digital voltage changes on the back panel, which indicate different traffic events in the field, to be captured by the data acquisition card installed in the industrial computer. A traffic event recorder software program, developed using the Microsoft Visual C# program, runs on the industrial computer in the field to record the events (for example, a phase 1 green change from “ON” to “OFF”) into a log file.

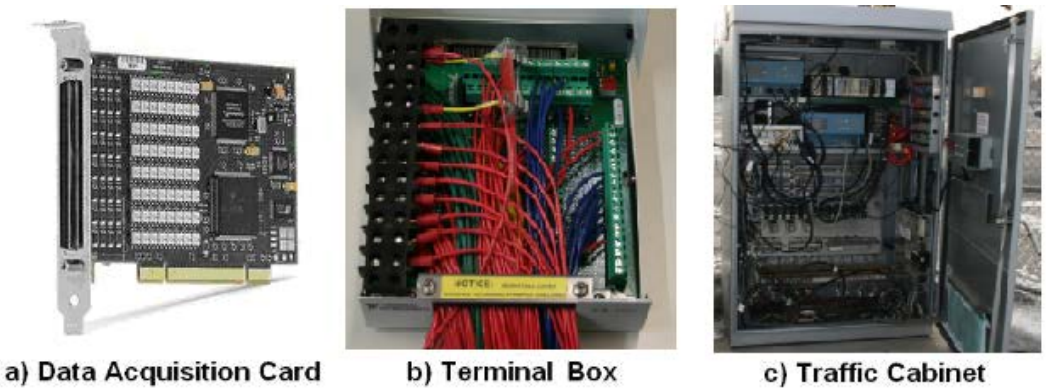

Figure 2.2 Demonstration of the Traffic Data Collection Components

Data communication between two controller cabinets is done using the existing twisted pair communication lines. A protocol of RS-485 is used to transmit data and synchronize time between cabinets (B&B Electronics, 2007). After the data in the local cabinets is transferred to the master cabinet, DSL or a wireless unit installed in the master cabinet is used to send the data back to the database located in the MTO in real time.

A sample of data is shown in Figure 2.3. Each logged event starts with a time stamp that includes the date, hour, minute, second and millisecond based on the computer system time, followed by different types of event data including phase changes, detector actuation and pedestrian calls. A complete history of traffic signal events is thus recorded.

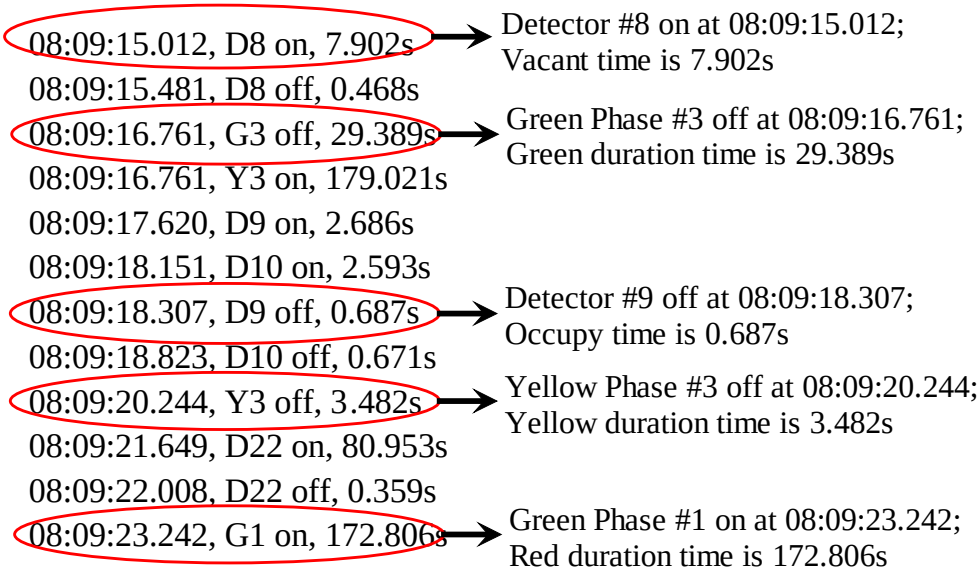

Figure 2.3 Sample Data (Source: Liu *et al.*, 2010)

2.3 Data Processing Procedure

The raw data collected from the field needs to be preprocessed and converted to an easy-read format before the performance measures can be derived. Based on event data, the signal phase duration can be calculated from the time difference between the start and end of a signal event.

The time interval between the start and end of a vehicle actuation event is the detector occupancy time, and the time interval between the end of a vehicle actuation event and the start of a following vehicle actuation event (from the same detector) is the time gap between two consecutive vehicles crossing the detector. Further processing can be done to determine second-by-second volume, occupancy, and cycle-by-cycle signal timing plan. The processed data can now be used to generate performance measures, such as queue length and average vehicle delay for intersections and travel time for arterial links. Figure 2.4 demonstrates the data flow of the SMART-SIGNAL system.

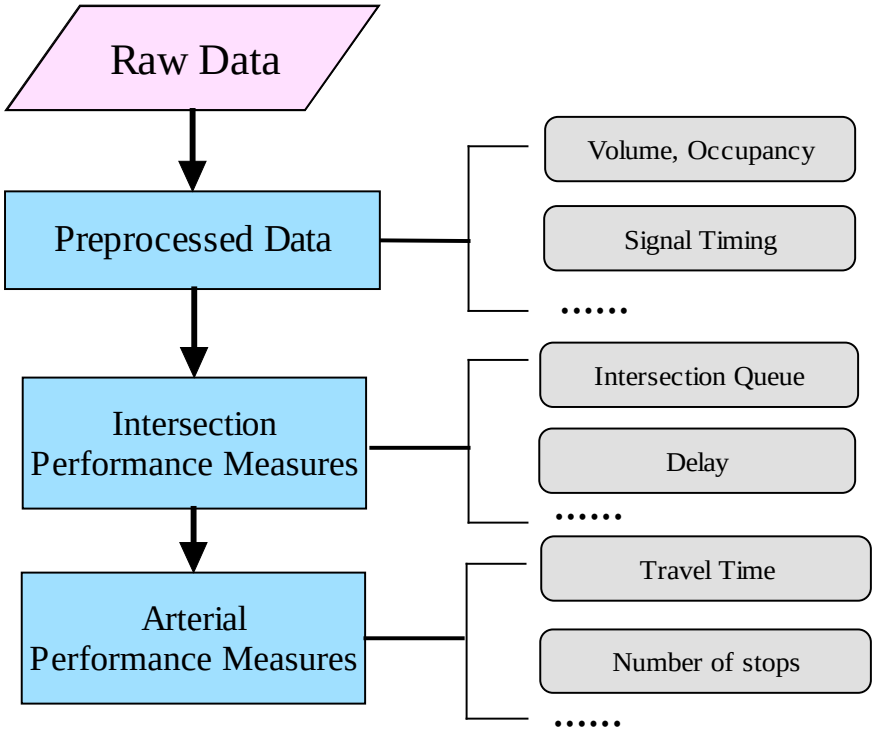

Figure 2.4 Data Flow of SMART-SIGNAL System (Source: Liu *et al.*, 2008)

Although many existing signal control systems are capable of generating data to support performance assessment, most do not make it "easy" for the managing agencies to prioritize improvements and plan for future needs. The SMART-SIGNAL System fills this gap. The high-resolution event data collected by the system is extremely valuable. The data is used to estimate real-time intersection queue length, identify queue spillover, and quantify the severity of oversaturation. In this research, the data is used to verify the accuracy of the SPM.

2.4 Virtual Probe Method

In this section, we briefly review the virtual probe based travel time estimation method. Interested readers should refer to Liu and Ma (2009) for further details.

To estimate real-time arterial travel time, in Liu and Ma (2009) we proposed a virtual probe approach by tracing an imaginary vehicle from origin to destination. Assume the journey of the virtual probe can be equally divided into many small time steps. At each time step, the states of

the virtual probe, including its position and speed, current signal status, and queue length ahead, are examined to determine the maneuver in the next time step. One of the three maneuvers, acceleration, deceleration or no-speed-change, is selected based on the current states of the virtual probe. The position and speed of the virtual probe at the next time step can then be calculated correspondingly. The step-by-step maneuver selection continues until the virtual probe "arrives" at the destination, and the difference between the starting time and the ending time is the arterial travel time. Detailed description of the virtual probe approach is provided in Liu and Ma (2009). Since the queue length ahead of the virtual probe is crucial for accurately estimating and predicting travel times, we will focus on the queue estimation in the rest of this report, particularly for the congested link with long queues.

Chapter 3. The Shockwave Profile Model

In this chapter, we present our SPM to describe the traffic flow dynamics within a signalized arterial link. For demonstration purposes, we use a simple one-way network with three signalized intersections *n-1*, *n*, and *n+1*, connected by two links with lengths L_n and L_{n+1} (Figure 3.1). Traffic in the minor streets is bi-directional with protected turnings. We will talk about how to deal with unprotected traffics later. We assume that traffic signal control parameters for all three intersections are known in advance for the time duration [*0*, *T*], where *T* is the ending time of simulation. For any time $t \in [0,T]$, we let $O_n(t)$ be the start time of the effective red in the current cycle for a movement of link L_n at intersection *n*, and let $r_n(t)$ and $g_n(t)$ be the effective red and green intervals in the current cycle for the same approach when time *t* belongs to the current cycle. In Figure 3.1, $q_{n-1}(t)$ represents the flow rate at the entrance of link L_n (i.e., inflow rate) at time *t*, and $\tilde{q}_n(t)$ and $\tilde{q}_n^m(t)$ the departure flow rates at intersection *n* (i.e. outflow rates) at time *t* from the major and minor approaches, respectively. Note $\tilde{q}_n^m(t)$ includes both the left and right turning traffics from the minor approaches (see Figure 3.1).

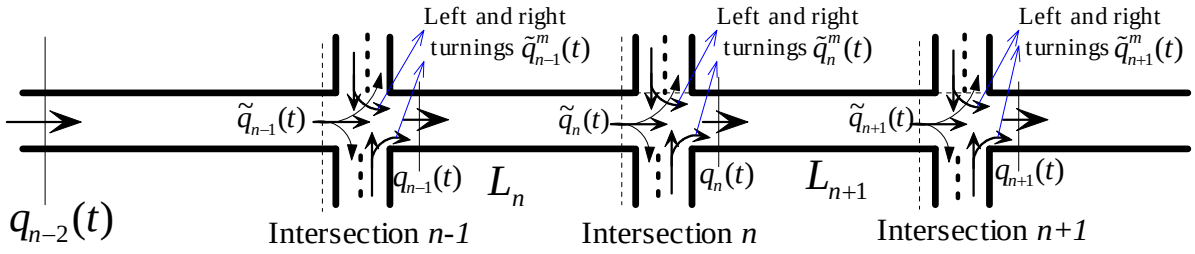

Figure 3.1 Layout of a Signalized Arterial with Three Intersections

To describe traffic flow dynamics, i.e., the trajectories of queue formation and dissipation on signalized links, we assume that the inflow rates at network boundaries are given. For a three-intersection network shown in Figure 3.1, inflow rates at network boundaries including $q_{n-2}(t), \tilde{q}_{n-1}^m(t), \tilde{q}_n^m(t)$, and $\tilde{q}_{n+1}^m(t)$ are assumed known. The initial condition of the network (i.e. traffic states within each link at the beginning) should also be given *a priori*. We now need to derive the outflow (i.e., $\tilde{q}_{n-1}(t), \tilde{q}_n(t)$, and $\tilde{q}_{n+1}(t)$) and inflow rates (i.e., $q_{n-1}(t), q_n(t)$, and $q_{n+1}(t)$) at all the intersections in addition to queue trajectories of each link. Note the input flow for downstream links $\left(q_{n-1}(t), q_n(t), \text{or } q_{n+1}(t)\right)$ is the sum of the discharge flows from the major and minor approaches, for example, for intersection *n*: $q_n(t) = \tilde{q}_n(t) + \tilde{q}_n^m(t)$. We should also note that in the SPM every signalized link is a section, within which the road segment is homogeneous with constant capacity. A link with turning bays or mid-block sinks and sources will be discussed in Chapter 4.

Similar to previous macroscopic traffic flow models, the foundation of SPM is the flow conservation law. For a signalized link L_n between time t_1 and t_2, assuming no sinks and sources between the link entry and exit, the following flow conservation equation holds:

$$\int_{t_1}^{t_2} q_{n-1}(t)dt + N_n(t_1) = \int_{t_1}^{t_2} \tilde{q}_n(t)dt + N_n(t_2) \quad (1)$$

where $N_n(t)$ is the number of vehicles within link L_n at time t. Note that, instead of using the differential form of the conservation law as most previous studies do, we use the integral form.

However, traffic dynamics cannot be fully described using solely the flow conservation equation. It must be supplemented by additional relations, such as the flow-density relation (i.e. the fundamental diagram) or a momentum equation describing the evolution of traffic speed. Our model, however, is built upon the observation that traffic dynamics at signalized intersections can be represented by a shockwave profile, which describes queue build-up and dissipation. Due to the cyclic disruption introduced by traffic lights, there exists a clear pattern of the first-order shockwaves at signalized intersections. These shockwaves clearly divide traffic states into free-flow, saturated, and jammed conditions. The SPM therefore takes advantage of the simplified traffic states to describe traffic dynamics based on a shockwave profile.

Consequently, the following assumptions are made in this report: **(1)** vehicles travel at free-flow speed before reaching the tail of a queue; **(2)** vehicles in a queue discharge at the saturation flow rate (when they are not constrained by downstream congestion); and **(3)** the velocity for a queue discharge shockwave is assumed to be known.

It is necessary to differentiate the above assumptions from those underlying the traditional fundamental diagram (FD), which hypothesizes a flow-density relationship. Assumption (1) actually indicates that the left hand side (uncongested area) in the FD is a straight line. This assumption is consistent with many empirical observations, i.e., vehicles are free-flow traveling when traffic is uncongested. The second and third assumptions imply known capacity and jam density, only two points in the FD. Except for these two points, the precise function of the congested regime for the FD does not need to be known. Indeed, till now, the exact shape of the right hand side of the FD is unknown, especially for signalized arterials (Wu et al., 2010b). Although much research has been devoted on this topic, whether it is linear (for example, the piecewise linear function applied in the CTM by Daganzo (1994 & 1995)), concave (for example, the parabolic function proposed by Greenshields (1935)), or some other form, is still an open question. The method presented here avoids this question by simplifying congested traffic conditions on an urban arterial into two states: saturated or jammed. These reasonable assumptions for traffic flow on a signalized link significantly simplify the model design and improve computational efficiency.

3.1 SPM for Intersections without Spillover from Downstream Links

The model for an individual intersection without downstream spillover is introduced in this chapter. Since SPM is built upon the cyclic shockwave profile on a signalized link, we start this chapter by reviewing the LWR shockwave equation. A shockwave is derived when applying the method of characteristics to analytically solve the partial differential equation (PDE) in the LWR

model. Basically, when characteristic curves (along which the density is constant) intersect, a shockwave is formed and wave velocity can be determined using Eq.(2):

$$w = \frac{q_b - q_a}{\rho_b - \rho_a} \tag{2}$$

where q_a (q_b) and ρ_a (ρ_b) are the traffic flow rate and density of upstream (downstream) respectively.

Due to the cyclic nature of signal phase changes, the shockwave profile at a signalized intersection also has a cyclic pattern. As indicated in Figure 3.2a, at the beginning of red (for better explanation, we assume there is no residual queue at the beginning of a cycle), a **queuing shockwave (w_1)** is generated and propagates backward. The queue reaches its maximum length when the queuing shockwave meets a **discharge shockwave (w_2)**, which also propagates backward from stop-bar after green light starts. As soon as these two waves meet, a third shockwave called a **departure wave (w_3)** is generated and propagates forward to the stop line. If a queue does not fully discharge by the end of cycle, a residual queue is formed (Figure 3.2b). The minimum queue will be achieved some time after the start of the red light for the next cycle when the departure wave meets a **compression wave (w_4)**. The compression wave has the same speed as the discharge wave, as both waves are generated from the discontinuity between the saturated and jammed traffic conditions. The velocities of all waves can be estimated using Eq.(2). Note that since arrival flows may vary along time, w_1 and w_3 may not be constant values. So the straight lines of w_1 and w_3 in Figure 3.2 are the simplified representations.

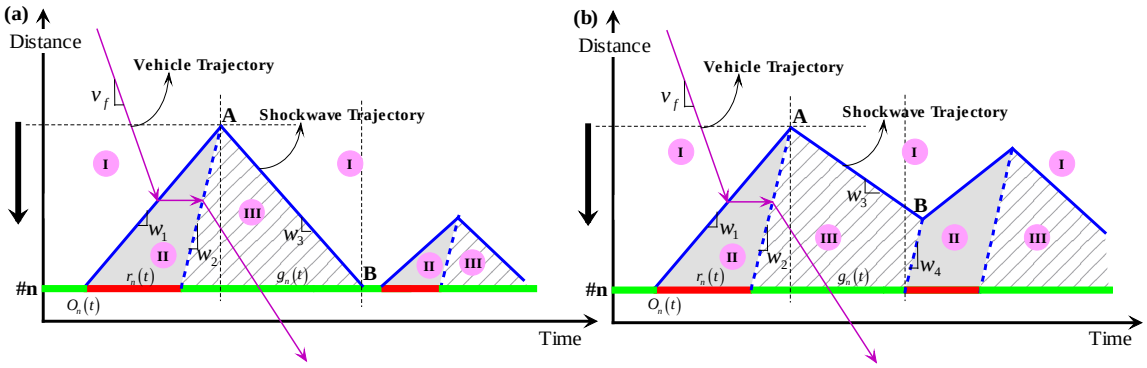

Figure 3.2 Shockwave Profile of Single Intersection: a) Without Residual Queues; b) With a Residual Queue

The fact that the shockwave pattern repeats from cycle to cycle makes them potentially very useful for simulating traffic dynamics in signalized networks. Specifically, a shockwave profile can be used to identify traffic states on a signalized link. Figure 3.2 shows the shockwave profiles of a single intersection with and without residual queues. In regime I of both diagrams, vehicles are free-flow traveling before reaching the front of a queuing wave w1 or departure wave w3. Since a linear flow-density relationship is assumed for uncongested traffic, the density in region I can be approximated by integrating traffic flow entering this area. Between the front of a queuing wave w1 (or compression wave w4, if there is a residual queue at the end of the previous cycle) and the stop line (or the front of a discharge wave w2), i.e., the shadowed region

II in the figure, vehicles cannot move and traffic density reaches the maximum (jam density). By contrast, in the shadowed region III, which is from the front of a discharge wave w2 and departure wave w3 to the stop line (or the front of a compression wave w4, if there is a residual queue at the end of the current cycle), vehicles are discharged at the saturation flow rate.

Before discussing the SPM, some important notations in this section are introduced below:

w: the velocity of a shockwave; there are four major shockwaves: queuing wave (w_1), discharge wave (w_2), departure wave (w_3), and compression wave (w_4);

$l_n^{w_j}(t)$: the distance from the front of shockwave w_j ($j = 1, 2, 3,$ or 4) to the stop line of intersection n at time t;

$l_n^{\hat{w}}(t)$: the queue length, defined as the distance from the front of shockwave w_1 or w_3 to the stop line at intersection n at time t, *i.e.*, $l_n^{\hat{w}}(t) = l_n^{w_1}(t)$ or $l_n^{w_3}(t)$, depending on which shockwave (w_1 or w_3) exists;

$r_n(t)$and $g_n(t)$: effective red and green intervals in the current cycle for a movement at intersection n when time t belongs to the current cycle;

v_f: free-flow speed.

S^n, ρ_j^n, and ρ_s^n: saturation flow rate, jam density, and saturation density at link L_n.

By integrating vehicles over a shockwave profile using Eq.(1) and applying the shockwave theory (Eq.(2)), the velocities of the four shockwaves w_1, w_2, w_3, and w_4 at time t can be derived based on the current signal status and locations of the shockwave fronts. w_2 and w_4 are easy to calculate since they separate the saturated and jammed traffic states, and the density and flow of these two states are given *a priori*. But for w_1 and w_3, we need to first estimate arrival flow and density, which depend on the input at the link entrance. Since we assume that vehicles are free-flow traveling before reaching the queue rear, for a queue with length ($l_n^{\hat{w}}(t)$), vehicles will take time $\frac{L_n - l_n^{\hat{w}}(t)}{v_f}$ traveling from the link entrance to the tail of the queue. So the arrival flow rate at the end of queue at time t is equal to the input flow rate at the link entrance at time $\left(t - \frac{L_n - l_n^{\hat{w}}(t)}{v_f}\right)$, and the arrival density becomes $q_{n-1}\left(t - \frac{L_n - l_n^{\hat{w}}(t)}{v_f}\right) \Big/ v_f$

Eq.(3)-(6) describe how to calculate the speeds of four waves.

Note that these four waves only exist within certain time ranges. For example, w_1 exists between the time when w_3 and w_4 meet with each other and the time when w_2 reaches w_1 (note if there is no residual queues, the start time of w_1 is the cycle start); and w_3 exists between the time when w_1 and w_2 meet with each other and the time when w_4 propagates back w_3 (similarly if there is no residual queues, the end time of w_3 is the cycle end). These intervals are determined by signal status and the time when other shockwaves meet with each other as described in Eq.(3)-(6).

$$w_1(t)=\begin{cases}\dfrac{-q_{n-1}\left(t-\dfrac{L_n-l_n^{\hat{w}}(t)}{v_f}\right)}{\rho_j^n-q_{n-1}\left(t-\dfrac{L_n-l_n^{\hat{w}}(t)}{v_f}\right)/v_f}, & \text{if } O_n(t)+\dfrac{l_n^{\hat{w}}(t)}{w^*}\le t<O_n(t)+r_n(t)+\dfrac{l_n^{\hat{w}}(t)}{w^*}\\ 0 & \text{otherwise}\end{cases} \tag{3}$$

$$w_2(t)=\begin{cases}-w^*, & \text{if } O_n(t)+r_n(t)\le t<O_n(t)+r_n(t)+\dfrac{l_n^{\hat{w}}(t)}{w^*}\\ 0, & \text{otherwise}\end{cases} \tag{4}$$

$$w_3(t)=\begin{cases}v_f, \text{ if } O_n(t)+r_n(t)+\dfrac{l_n^{\hat{w}}(t)}{w^*}\le t<O_n(t)+r_n(t)+g_n(t) \text{ or } O_n(t)\le t<O_n(t)+\dfrac{l_n^{\hat{w}}(t)}{w^*}\\ 0, \quad \text{otherwise}\end{cases} \tag{5}$$

$$w_4(t)=\begin{cases}-w^*, & \text{if } O_n(t)\le t<O_n(t)+\dfrac{l_n^{\hat{w}}(t)}{w^*}\\ 0, & \text{otherwise}\end{cases} \tag{6}$$

where w^* is a constant and can be calculated by Eq. (7):

$$w^*=\frac{S^n}{\rho_j^n-\rho_s^n}. \tag{7}$$

We should also note that, if the discharging flow rate after green light starts is lower than the maximum arrival rate at free-flow condition, i.e., the existence of capacity drops as found in many empirical studies (for example: Koshi et al., 1983; Hall et al., 1986), the value of w_3 may not be a free-flow speed but can be calculated by Eq.(8).

$$w_3(t)=\begin{cases}\dfrac{S^n-q_{n-1}\left(t-\dfrac{L_n-l_n^{\hat{w}}(t)}{v_f}\right)}{\rho_s^n-q_{n-1}\left(t-\dfrac{L_n-l_n^{\hat{w}}(t)}{v_f}\right)/v_f}, & \text{if } O_n(t)+r_n(t)+\dfrac{l_n^{\hat{w}}(t)}{w^*}\le t<O_n(t)+r_n(t)+g_n(t)\\ & \text{or } O_n(t)\le t<O_n(t)+\dfrac{l_n^{\hat{w}}(t)}{w^*}\\ 0, & \text{otherwise}\end{cases} \tag{8}$$

Based on the values of $w_1(t)$ and $w_3(t)$ and the current queue length ($l_n^{\hat{w}}(t)$), the queue length at the next time step ($t+\Delta t$), i.e., $l_n^{\hat{w}}(t+\Delta t)$, can be updated using Eq.(9). Note that the distance should be neither negative nor longer than the link length.

$$l_n^{\hat{w}}(t+\Delta t)=\begin{cases}\min\left\{L_n,\max\left\{0,l_n^{\hat{w}}(t)-w_1(t)\cdot\Delta t\right\}\right\}, & \text{if } w_1(t)\neq 0\\ \min\left\{L_n,\max\left\{0,l_n^{\hat{w}}(t)-w_3(t)\cdot\Delta t\right\}\right\}, & \text{if } w_3(t)\neq 0\\ \min\left\{L_n,\max\left\{0,l_n^{\hat{w}}(t)\right\}\right\}, & \text{otherwise}\end{cases} \tag{9}$$

Similarly, based on the values of $w_2(t)$ and $w_4(t)$, and the current wave front positions of w_2 and w_4 ($l_n^{w_2}(t)$ and $l_n^{w_4}(t)$), the wave front positions at the next time step ($t+\Delta t$), i.e., $l_n^{w_2}(t+\Delta t)$ and $l_n^{w_4}(t+\Delta t)$, can be updated using Eq.(10):

$$l_n^{w_j}(t+\Delta t)=\begin{cases}\min\left\{L_n,\max\left\{0,l_n^{w_j}(t)-w_j(t)\cdot\Delta t\right\}\right\}, & \text{if } w_j(t)\neq 0\\ 0, & \text{otherwise}\end{cases},\ j=2 \text{ or } 4 \tag{10}$$

It should be pointed out that here we assume a constant rate of arrival within each Δt. So the wave fronts of w_1 and w_3 would form two piecewise linear curves. When Δt is large and the arrival pattern changes drastically within each Δt, this could result in significant estimation errors.

Once the wave positions are updated, the shockwave profiles can be constructed. These profiles are then used to determine the outflow from an intersection: if the signal is red, the outflow rate is zero; when the signal turns green, the departure rate is equivalent to the saturation rate if there is a queue, or determined by the arrival flow with a time lag (L_n/v_f) after the queue has been fully discharged. Considering that the intersection output may also be constrained by the downstream capacity, the following equation summarizes the results:

$$\tilde{q}_n(t)=\begin{cases}0, & \text{if } O_n(t)\le t<O_n(t)+r_n(t)\\ \min\left\{S^n,S^{n+1}\right\}, & \text{if } O_n(t)+r_n(t)\le t<O_n(t)+r_n(t)+g_n(t)\ \&\ l_n^{\hat{w}}(t)>0\\ \min\left\{q_{n-1}\left(t-\dfrac{L_n}{v_f}\right),S^{n+1}\right\}, & \text{if } O_n(t)+r_n(t)\le t<O_n(t)+r_n(t)+g_n(t)\ \&\ l_n^{\hat{w}}(t)=0\end{cases} \tag{11}$$

However, Eq.(11) only works for approaches with protected signal phases. For unprotected approaches, the output flow rates are also constrained by the availability of acceptable gaps in the conflicting approach as shown in Figure 3.3. We assume the availability of acceptable gaps is proportional to the spare capacity, i.e., the difference between the maximum flow rate and the current discharge rate on the conflicting approach. Here γ is introduced as the proportional

constant with a value between 0 and 1. $\gamma = 0$ means that none of the spare capacity can be used to discharge vehicles on an unprotected approach, while $\gamma = 1$ means the opposite. Parameter γ is assumed to be given *a priori*. Intuitively, γ becomes smaller when the number of lanes on the conflicting approach increases, and γ is smaller for an unprotected left turn (a) than that for an unprotected right turn (Figure 3.3b). Assuming a known γ, we should use the Eq.(12), instead of Eq.(11), to calculate the output flow rates for unprotected approaches.

$$\tilde{q}_n(t) = \begin{cases} 0, & \text{if } O_n(t) \le t < O_n(t) + r_n(t) \\ \min\left\{\gamma\left(S^{cfl} - \tilde{q}_n^{cfl}(t)\right), S^n, S^{n+1}\right\}, & \text{if } O_n(t) + r_n(t) \le t < O_n(t) + r_n(t) + g_n(t) \;\&\; l_n^{\hat{w}}(t) > 0 \\ \min\left\{\gamma\left(S^{cfl} - \tilde{q}_n^{cfl}(t)\right), q_{n-1}\left(t - \dfrac{L_n}{v_f}\right), S^{n+1}\right\}, & \text{if } O_n(t) + r_n(t) \le t < O_n(t) + r_n(t) + g_n(t) \;\&\; l_n^{\hat{w}}(t) = 0 \end{cases} \quad (12)$$

where $S^{cfl}(t)$ and $\tilde{q}_n^{cfl}(t)$ are the saturation flow rate and discharge flow rate on a conflicting approach; and $\tilde{q}_n(t)$ represents the discharge flow rate from an unprotected approach.

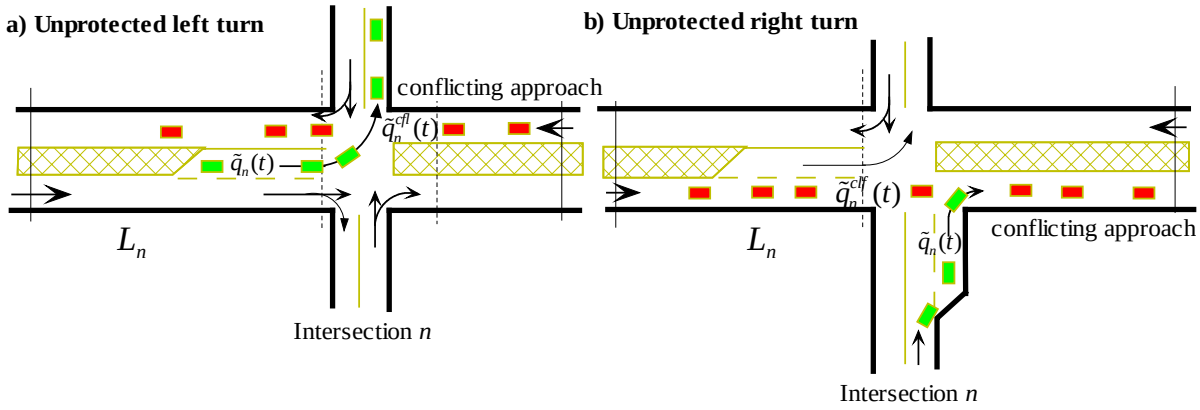

Figure 3.3 Outputs for Unprotected Approaches

Also, for unprotected approaches, since traffic in a queue may not be discharged at the theoretical saturation flow rate due to a conflicting flow, the saturation flow used in Eq.(3)-(7) should be changed to a feasible discharge flow rate, which is constrained by the spare capacity of the conflicting link. So we use Eq.(13) to estimate the actual saturation flow rate for unprotected traffics. This value will replace the theoretical one in Eq.(3)-(7) for unprotected approaches.

$$S_n^A(t) = \min\left\{\gamma\left(S^{cfl} - \tilde{q}_n^{cfl}(t)\right), S^n\right\} \quad (13)$$

where $S_n^A(t)$ is the actual saturation flow rate for an unprotected approach; and S^n is the theoretical value without the impact from conflicting flows.

After deriving the output from the upstream intersections, the input for the downstream intersections can be easily derived given a known turning percentage (β_n) for the through movement at link L_n:

$$q_n(t) = \begin{cases} \tilde{q}_n^m(t), & \text{if } O_n(t) \le t \le O_n(t) + r_n(t) \\ \beta_n \cdot \tilde{q}_n(t), & \text{if } O_n(t) + r_n(t) < t \le O_n(t) + r_n(t) + g_n(t) \end{cases} \quad (14)$$

where $\tilde{q}_n^m(t)$ is the departure flow rate of minor streets (including both left and right) at intersection *n*.

3.2 SPM for Intersections with Spillover from Downstream Links

For multiple intersections, the main issue is how to deal with spillover from downstream traffic. When a spillover from downstream happens, the cyclic process of queue build-up and dissipation is disturbed. The shockwave profile for an urban network with more than one intersection could be very complicated. Depending on when spillover occurs and how long spillover lasts, the effects of spillover are equivalent to either extending the original red time or creating new small cycles, as described in the following:

Case I: Extending the red phase. The first case, as presented in Figure 3.4a, describes a situation in which when the queue at downstream intersection (*n+1*) spills back to upstream intersection (*n*), the signal at intersection *n* is red, and the spillover persists after the signal turns green. In this case, vehicles cannot be discharged when the signal turns green until a discharge wave generated at the downstream intersection propagates back to the upstream intersection. It is equivalent that the red phase has been extended to the time when the discharge wave arrives.

Case II: Creating a new cycle. Unlike Case I, the second case represents a situation that when the queue from the downstream intersection (*n+1*) spills back to the upstream intersection (*n*), the signal at the upstream intersection is green (Figure 3.4b). Vehicles are forced to stop until the discharge wave generated at the downstream intersection propagates back the upstream intersection, rendering a portion of the green time unusable. As shown in Figure 3.4b, once spillover happens, a compression wave (w_4) is generated at the n^{th} intersection; this wave propagates backward and will meet the original departure wave (w_3), creating a new queuing wave (w_1). Note that if the queue at the n^{th} intersection has been fully discharged before the spillover occurs, a new queuing wave (w_1), not a compression wave (w_4), will be generated. When the spillover dissipates, a new discharge wave (w_2) will be generated, propagating backward and eventually meeting up with the new queuing wave (w_1). The structure of this shockwave profile becomes much more complex compared with those without spillover. However, as clearly indicated in Figure 3.4b, spillover essentially creates a new cycle, in which the new red phase starts when spillover occurs and ends when the discharge wave from downstream intersection arrives at the upstream intersection. Within the new cycle, the shockwave profile presents the same pattern as described in Figure 3.2 for the situation without spillover.

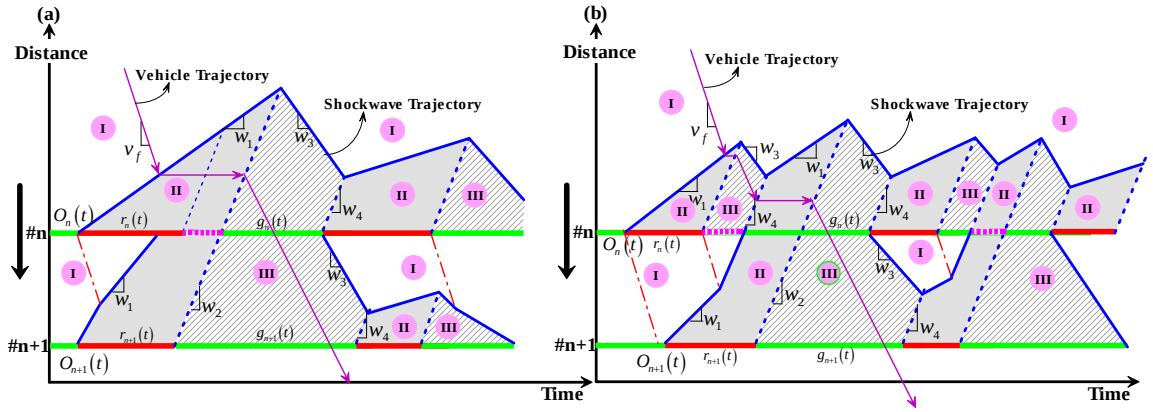

Figure 3.4 Two Interpretive Cases for Spillover:
a) I: Extending the Red Phase; b) II: Creating a New Cycle

It turns out that for multiple consecutive intersections along an arterial, the impact of spillover can also be described by extending a red phase or creating new cycles. See the two examples for three intersections in Figure 3.5, spillover from intersection *n+1* first changes the signal timing at intersection *n* by either extending a red phase (Figure 3.5a) or creating a new cycle (Figure 3.5b); and then spillover created by the new signal timings at intersection *n* impacts intersection *n-1* by either extending a red phase (Figure 3.5a) or creating new cycles (Figure 3.5b). Since the effect of spillover between any two adjacent intersections can be described, spillover in a complicated large network, which consists of many intersections, can be simply treated as either extending red phases or creating small cycles.

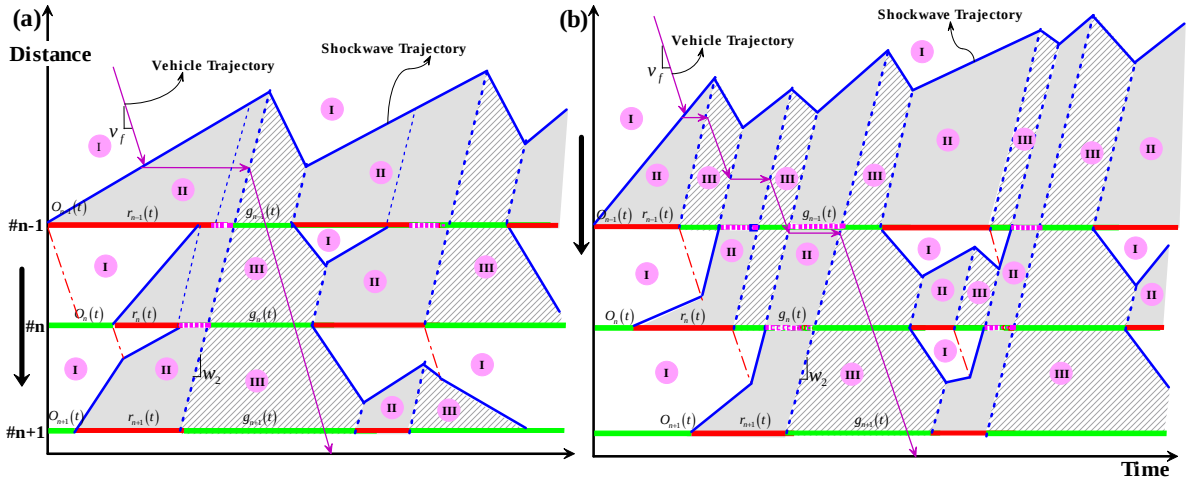

Figure 3.5 Shockwave Profiles for Three Intersections with Spillovers

Figure 3.4 & Figure 3.5 also indicate the traffic states along an arterial link. As described before, we categorize traffic conditions on an arterial into three states: free-flowing, saturated, and jammed; and SPM only captures the dynamics for four major shockwaves. But it should be clarified here that there are many other waves besides these four waves. As indicated in Figure 3.4 & Figure 3.5, right after signal changes from green to red, a wave, as marked by a red dash-dot line, may be generated due to the change of discharge flow rate. The wave propagates forward and may meet a queuing wave and change its velocity as indicated by the slope changes

of queuing waves in Figure 3.4 & 5. However, as claimed in the beginning of this report, the key for modeling traffic dynamics on signalized arterials is to describe queue formation and dissipation, which are captured by four major waves. Other waves do not necessitate explicit formulation. For example, by simply assuming that vehicles travel at free-flow speed before reaching a queue, SPM can estimate the exact time and location of the slope change in a queuing wave caused by a forward wave generated right after signal turns green without tracing the forward wave.

Since spillover can be treated as either extending a red phase or creating new cycles, to deal with spillover, we update signal timing at the time when a queue spills back to the upstream intersection (i.e., $l_{n+1}^{\hat{w}}(t) < L_{n+1} \le l_{n+1}^{\hat{w}}(t+\Delta t)$ or $l_{n+1}^{w_4}(t) < L_{n+1} \le l_{n+1}^{w_4}(t+\Delta t)$) and when a discharge wave propagates back to the upstream (i.e. $l_{n+1}^{w_2}(t) < L_{n+1} \le l_{n+1}^{w_2}(t+\Delta t)$). However, since SPM updates traffic states at each time instant *t*, when spillover happens, the duration of spillover is not known. For modeling convenience, we treat the rest of the time in the cycle as red when spillover happens, and let the rest of the time in the cycle as green when spillover dissipates. Note that it is possible to have a situation in which the signal is red when the discharge wave (w_2) propagates back to the upstream intersection. For this situation, we cannot set the remaining time in the cycle as green; instead, the remaining red is considered as the new red period and the green remains the same. Eq.(15) summarizes all situations.

$$\begin{cases} \text{if } l_{n+1}^{\hat{w}}(t) < L_{n+1} \le l_{n+1}^{\hat{w}}(t+\Delta t) \\ \text{or } l_{n+1}^{w_4}(t) < L_{n+1} \le l_{n+1}^{w_4}(t+\Delta t) \end{cases} \text{ then } \begin{cases} O_n(t+\Delta t) = t \\ r_n(t+\Delta t) = O_n(t) + r_n(t) + g_n(t) - t \\ g_n(t+\Delta t) = 0 \end{cases} \\ \text{if } l_{n+1}^{w_2}(t) < L_{n+1} \le l_{n+1}^{w_2}(t+\Delta t) \text{ then } \begin{cases} O_n(t+\Delta t) = t \\ r_n(t+\Delta t) = \max\{O_n(t) + r_n(t) - t, 0\} \\ g_n(t+\Delta t) = O_n(t) + r_n(t) + g_n(t) - r_n(t+\Delta t) - t \end{cases} \end{cases} \quad (15)$$

Note that by comparing $(O_n(t) + r_n(t) - t)$ and *0*, we can determine whether there is red time left when discharge wave (w_2) arrives.

Once the signal status is updated, the model introduced in the last section can be applied to describe traffic dynamics with spillover. As we noted earlier, the shockwave profiles with spillover for multiple intersections are extremely complicated. Figure 3.5 presents two potential shockwave profiles for an arterial with three intersections, but there are many other possible profiles depending on when spillover happens, how long spillover lasts, and whether there is a residual queue at the end of the cycle. It is infeasible to enumerate all the possible profiles and apply the model described in Chapter 3.1 to estimate the traffic dynamics. However, all spillovers can be categorized as extending a red phase (case I) or creating new cycles (case II). Complicated scenarios with spillover can then be converted to cases without spillover by updating signal timings using Eq.(15). This is tremendously beneficial for large network

applications since the simple model introduced for non-spillover situations can be directly applied no matter how complicated the shockwave profiles are.

Chapter 4. Network Representation

4.1 Nodes and Arcs

To complete the model, we need to choose an appropriate method to represent an arterial network. Since SPM treats each homogeneous road segment as a section, it is convenient to use nodes to represent road sections with arcs between two adjacent nodes to indicate the direction of vehicle transfer. Here nodes carry most of the physical data including arterial link lengths, parameter values (such as jam density, saturation rate, etc.), and signal timing plans. The data is then used to construct shockwave profiles, to derive potential departure rates, and to determine arrivals for downstream nodes. Arcs, by contrast, play only a minor role, as they simply indicate travel directions to ensure vehicles are properly transferred among nodes. Figure 4.1 gives an example of a single intersection represented by nodes and arcs.

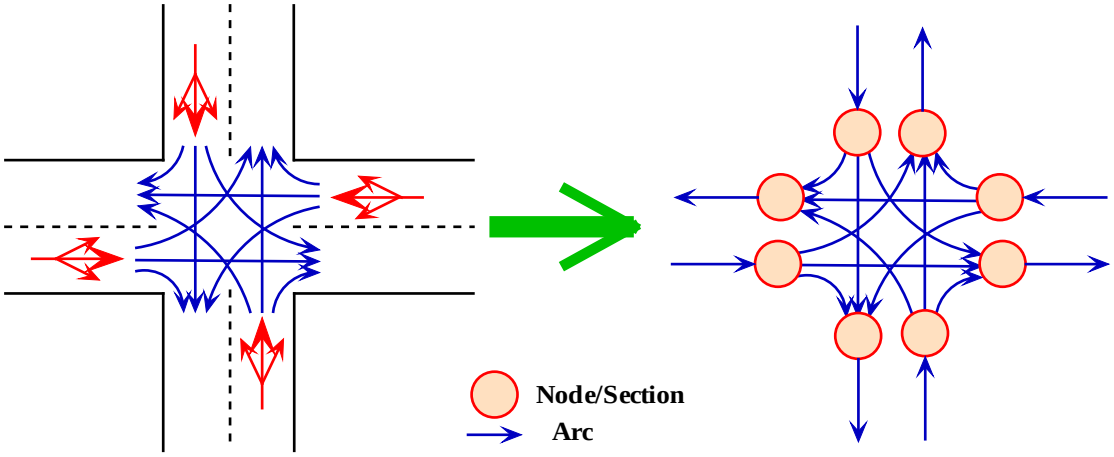

Figure 4.1 Nodes and Arcs

Note that a signal link should be subdivided into sections if the number of lanes changes, since new shockwaves may be generated at the location where traffic heterogeneity exists. The connecting point between two consecutive sections is modeled as a virtual intersection with an all-green phase. The model introduced in Chapter 3 can then be applied.

4.2 Network Representations for Intersections with Turning Bays

One case we have not addressed yet in our model is intersections with turning bays. A signal link with turning bays cannot be treated simply as two sub-sections because turning movements may have separate signal control with through movement, and more importantly, spillover from turning bays may lead to the blockage of through movement. In order to apply the SPM model described in Chapter 3, we divide the link into three sections as shown in Figure 4.2a: L_n^U, L_n^B, and L_n^A, representing upstream through movement (starting from the link entrance to the separation point U), downstream through movement (starting from the separation point U to the stop line), and turning bays, respectively (note $L_n^B = L_n^A$). These three sections are represented by three nodes as described in Figure 4.2b. Separation point U is treated as a virtual intersection

with all-green, as shown in Eq.(16). The equations presented in Chapter 3 can then be applied. Note Eq.(11) and (13) shall be used if turning traffic is not protected.

$$\begin{cases} O_n(t) = 0 \\ r_n(t) = 0 \\ g_n(t) = T \end{cases} \tag{16}$$

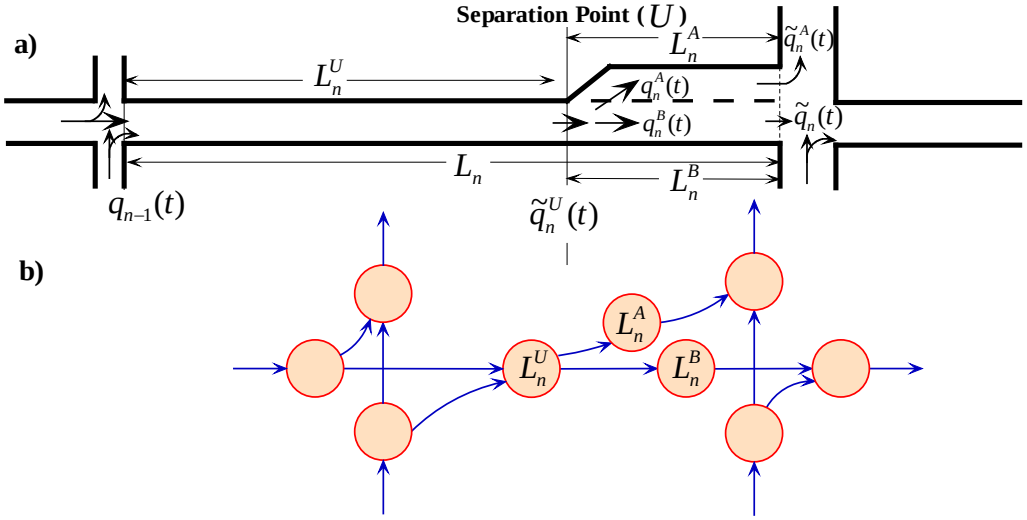

Figure 4.2 a) Layout of an Intersection with Turning Bay; b) Network Representation

An example of a shockwave profile for a signal link with turning bay is shown in Figure 4.3. When the queuing wave on the turning section $L_n{}^A$ (represented by the purple star line) propagates back to the separation point U, a shockwave profile on section $L_n{}^U$ (represented by the dark blue solid line) is generated. Meanwhile the shockwave profile on section $L_n{}^B$ (represented by the light green dash-dot line) has also been impacted since there are no more vehicles coming from upstream.

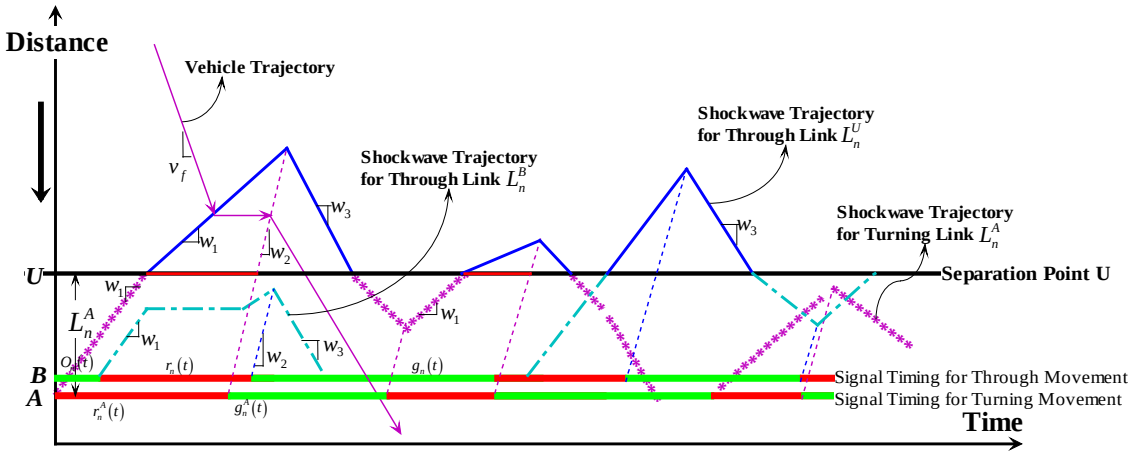

Figure 4.3 Shockwave Profiles for an Intersection with Spillover at Turning Bays

We should note that if section L_n^U has multiple lanes, it is not uncommon that only the leftmost lane on L_n^U is blocked and the other lanes remain open when a queue spills back from turning bay L_n^A to the separation point U (see Figure 4.4a). Under such circumstances, section L_n^U needs to be split into two parallel sub-sections, L_n^{V1} and L_n^{V2}, representing the blocked and unblocked lanes separately (see Figure 4.4b). The inputs for the two sub-sections ($q_n^{V1}(t)$ and $q_n^{V2}(t)$) are assigned directly at the entrance of section L_n^U based on known turning percentages; and the output is determined by the signal timings at two virtual intersections (i.e. points V_1 and V_2) and shockwave profiles in two sub-sections L_n^{V1} and L_n^{V2}. Here we need to introduce a dummy node (with zero section length) to represent traffic flow coming from upstream intersections before we split section L_n^U into the two sub-sections based on the turning percentage (see Eq.(17)).

$$\begin{cases} q_n^{V1}(t) = (1-\beta_n)\cdot q_{n-1}(t) \\ q_n^{V2}(t) = \beta_n \cdot q_{n-1}(t) \end{cases} \tag{17}$$

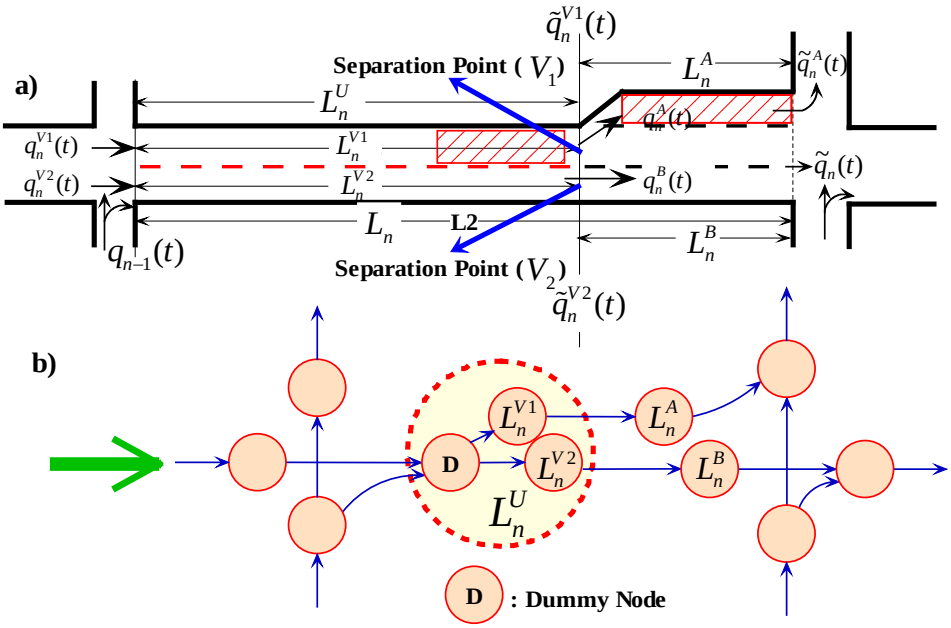

Figure 4.4 Layouts of Intersections with Turning Bays – Through Movements are Partially Blocked

It should be known that the lane-based section design is only an approximation of the real world. We assume that vehicles have been assigned to different lanes (or lane groups) at the entrance of the link in order to avoid dealing with complex lane-changing behaviors. Although this assumption is not exactly true, it is still a reasonable one as when one lane is blocked, it is very likely that vehicles will make a lane choice earlier. Although a more sophisticated lane-changing model may increase accuracy, it also comes with higher computational cost. The model we propose is more numerically efficient and robust, and thus more appropriate for large arterial network applications.

4.3 Network Representations for Links with Mid-block Sinks and Sources

If we know arrival flow rates from mid-block sources and turning percentages for mid-block sinks, traffic dynamics can be described by further separating a link with a mid-block source (or sink) into two sub-sections: $L_n^{\ 1}$ and $L_n^{\ 2}$, representing an upstream section before a mid-block source (or sink) and a downstream section after mid-block, respectively. Figure 4.5a presents a small network with a sink and a source on two links. The corresponding network representation is presented in Figure 4.5b. A virtual intersection with all-green is assumed at the merging (or diverging) point at mid-block. Since vehicles have to find acceptable gaps to merge into the objective link, Eq.(12) and (13), which are designed to simulate traffic behaviors for left/right turnings with unprotected phases, are applied to describe wave propagations.

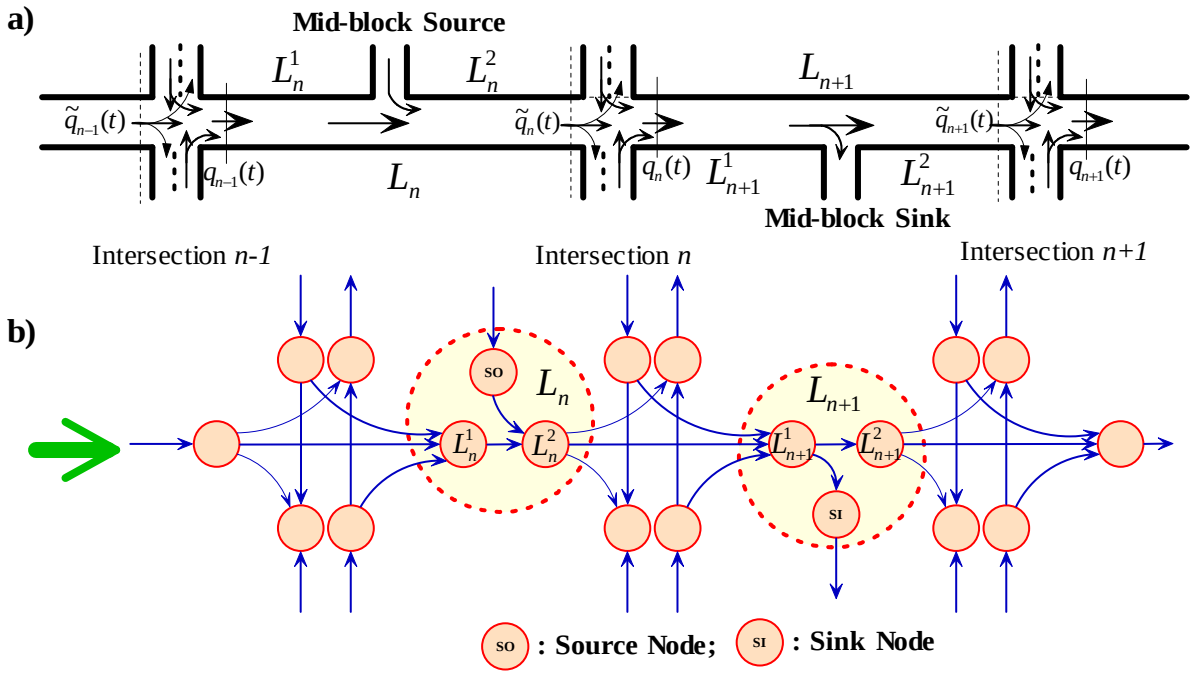

Figure 4.5 a) An Arterial with Mid-block Sinks and Sources; b) Network Representation

Chapter 5. Numerical Example: SPM vs. CTM

In this chapter, we provide a small numerical example to demonstrate the capability of SPM. In particular, the results estimated by SPM were compared with those generated from CTM. For this experiment, we used a simple arterial with two intersections and two links but no turning movements, as shown in Figure 5.1a. The second link was designed relatively short in order to create spillover. The model inputs, including arrival flow at the entrance of the first intersection, signal timings, free-flow speed, jam density, discharge wave velocity, saturation flow, and flow-density relation for CTM, are presented in Figure 5.1b-d.

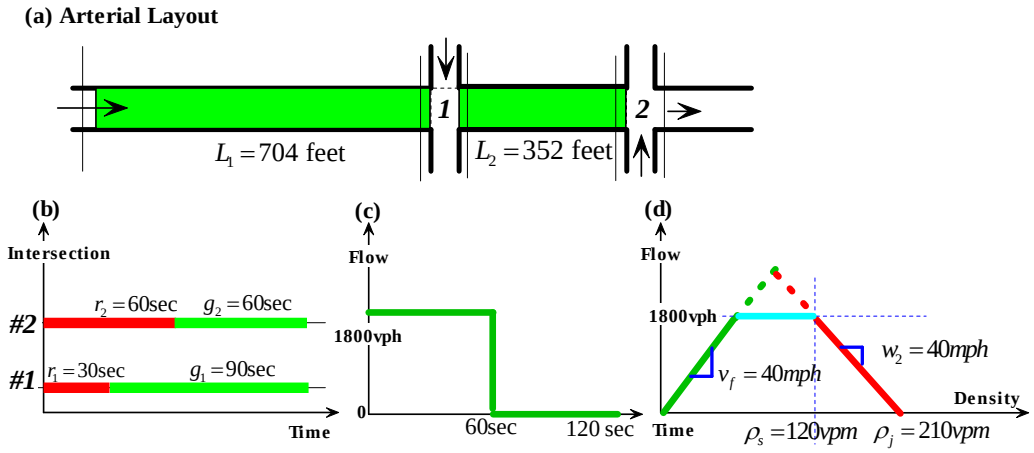

Figure 5.1 a) Layout of the Two-intersection Example, b) Signal Timing Parameters, c) Input Flow Rate, and d) The Dundamental Diagram

5.1 Cell Design for CTM and Section Design for SPM

We first briefly discuss CTM and its cell design. CTM applies the following equations for the simulation of traffic dynamics:

$$\begin{cases} x_i(t+1) = x_i(t) + f_i(t) - f_{i+1}(t) \\ f_i(t) = \min\left\{ x_{i-1}(t), Q_i(t), (\frac{w}{v_f}) \cdot \left[Z_i(t) - x_j(t) \right] \right\} \end{cases} \tag{18}$$

where $x_i(t)$, $f_i(t)$, $Q_i(t)$, and $Z_i(t)$ denote the number of vehicles, the actual inflow, the inflow capacity (the maximum allowable inflow), and the holding capacity (the maximum allowable number of vehicles) in cell i at time t. Essentially, the first equation describes the flow conservation for each cell; and the second represents the possible number of vehicles entering a cell based on a hypothesized piecewise linear fundamental diagram.

One of the most important steps in CTM is to discretize links into homogenous cells such that the cell length is equal to the distance traveled by a free-flowing vehicle in one time interval. Generally, CTM will generate more accurate results when cell length is relatively short. In this example, we use a one-second time interval and a cell length is 58.67 feet under the assumption

that the free-flow speed is 40 mph. Figure 5.2a presents the cell design for the two-link arterial. Note that the last cell (the blue one) has infinity holding capacity so that the departure from the upstream cell is not restricted. Compared with the section design for SPM (see Figure 5.2b), the cell design for CTM is much more complicated.

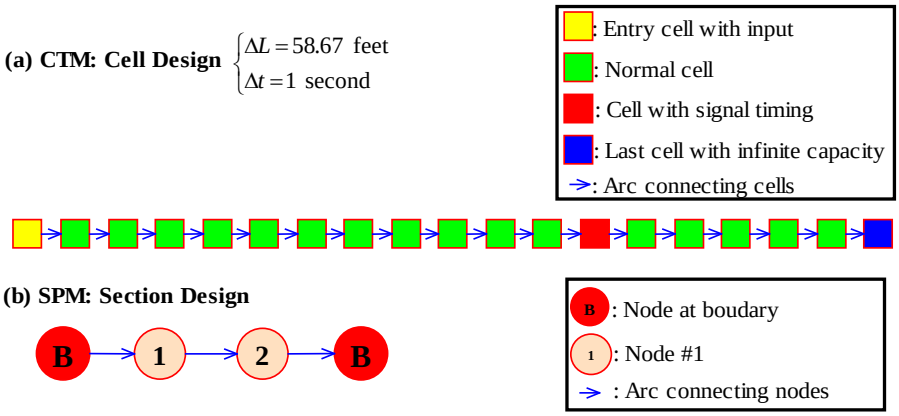

Figure 5.2 Cell Design for CTM and Section Design for SPM

5.2 Results

The results presented here are only for the first link (L_1 = 704ft) from one of the signal cycles. Since CTM estimates the density for each cell at each time interval, we show the density contour in Figure 5.3a. Figure 5.3b displays the corresponding shockwave profile generated by SPM. As can be seen, the shockwave profile closely matches the density contour from CTM. Figure 5.4 presents the output flow from the stop-bar at the first intersection for both models. These results are also very consistent. Note that a downstream spillover occurs in this cycle and the purple dash bar represents the updated red phase due to spillover.

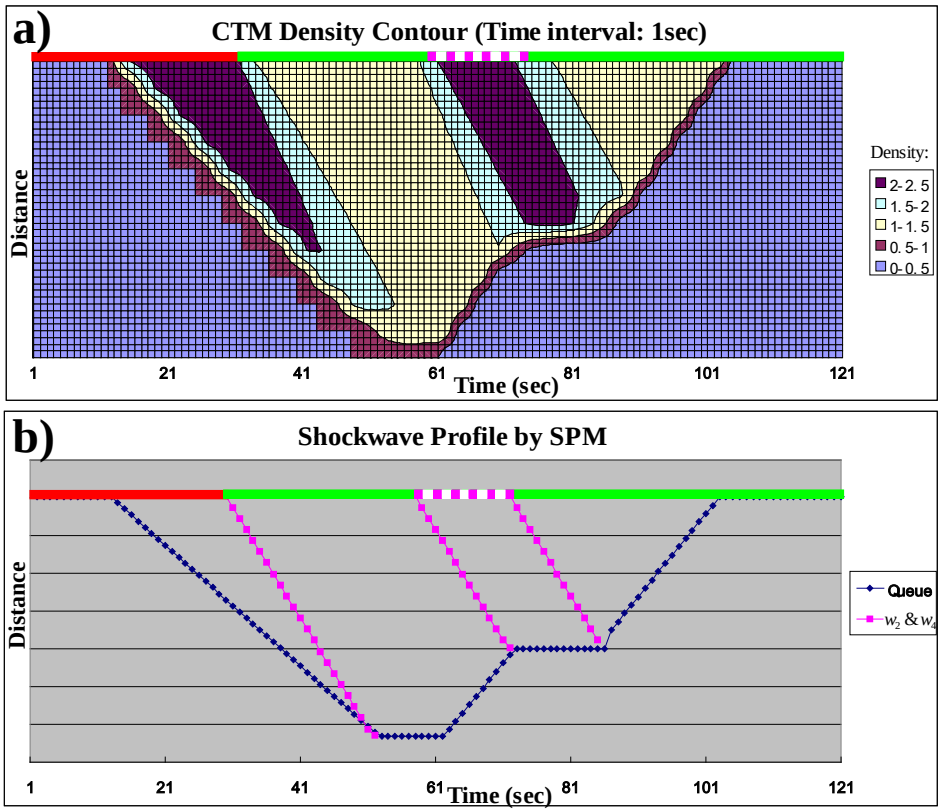

Figure 5.3 a) CTM Density Contour (Time Interval: 1 sec); b) Shockwave Profile Generated by SPM.

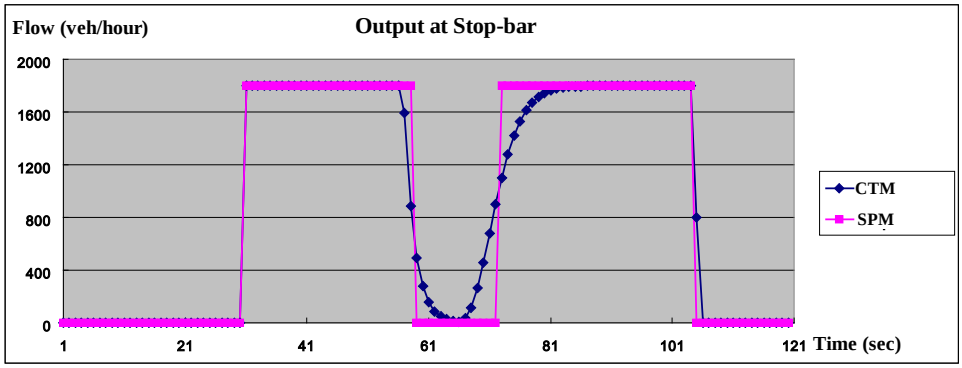

Figure 5.4 Output at the Stop-bar for the First Intersection

Chapter 6. Field Test Results

6.1 Field Data Collection

We further validated the SPM model using the field data collected from Trunk Highway 55 (TH55), a major arterial in the Twin Cities, Minnesota. For the purpose of signal operation, advance detectors are installed for major approaches (about 400 feet upstream from the stop line) to detect vehicles for green extension; and stop-bar detectors installed on minor streets (right behind the stop line) to detect the presence of vehicles. For research purposes, we also installed stop-bar and link entrance detectors on major approaches. Figure 6.1 shows the detector configurations for three intersections (Winnetka Ave., Rhode Island Ave., and Glenwood Ave.). We do not include the advance detectors in the figure since no information from them was used in this study.

All three intersections are installed with the SMART-Signal system, which continuously collects and archives high-resolution event-based traffic signal data in real time. The event data provide start and end times of each vehicle-detector actuation and signal phase change, making it possible to extract time-dependent traffic volume, turning percentage, and signal phase information at each intersection from the raw data.

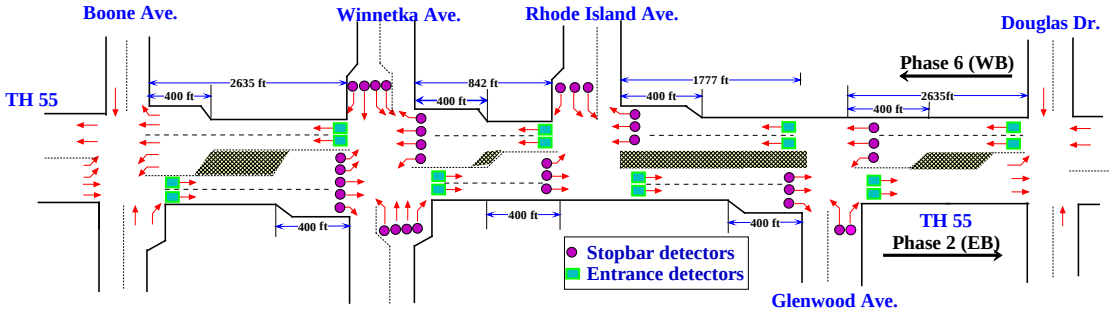

Figure 6.1 Layout of TH55 Test Site

The data we selected to test the model was collected during an afternoon peak on Nov. 17, 2008. The day was specifically selected because a nine-cycle spillover was known to have occurred between 17:06:31 and 17:36:31 at the westbound of the intersection TH55/Rhode Island Ave., as shown in our previous research (see Wu et al., 2010a for a detailed discussion of spillover and oversaturation). The input data to the SPM model included the time-dependent traffic volume at the arterial boundaries, the turning percentage at each intersection, and the signal phase information for each approach. The inflow at the boundaries was collected by the entrance detectors at the eastbound link of the intersection of Winnetka Ave. and the westbound link of the intersection of Glenwood Ave., and by the stop-bar detectors at all minor streets (see Figure 6.1).

6.2 Network Representation

The three intersections of interest on TH55 are represented as a network in Figure 6.2. Since there are turning bays, each link between two intersections is divided into four sections

represented by four nodes and four arcs. The start or end nodes at boundaries are treated as dummy nodes, which have infinity lengths to store vehicles.

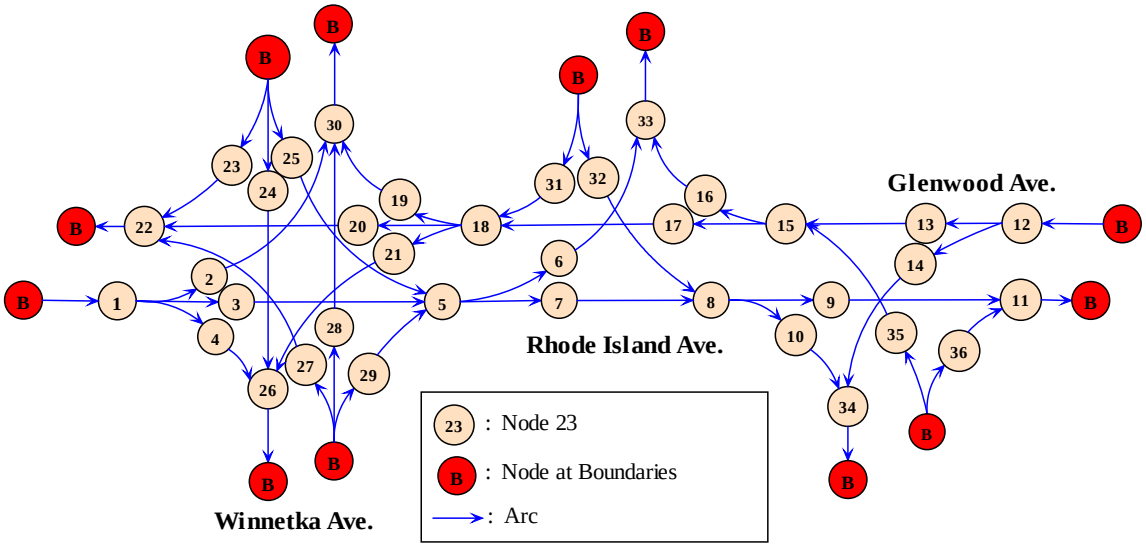

Figure 6.2 Network Representation for the Three Intersections on TH55

6.3 Results

We use SPM to simulate traffic dynamics for three hours (16:00:00 -19:00:00), but only two hours of data (16:30:00 -18:30:00) for the westbound of TH55 are presented here for demonstration purposes. In this study, the saturation flow rate, free flow speed, and jam density were set to 2100 veh/hr/ln, 45 mile/hr, and 176 veh/mile/ln, respectively. Consequently, the discharge shockwave speed used in this report was 16.2 mile/hr. These parameters were estimated using the high-resolution data collected from the SMART-Signal system. Since only right turning traffics are unprotected, γ was set to 1.The time interval we used for SPM was one second.

Figure 6.3 and Figure 6.4 compare the simulated traffic volumes with the ground truth collected by the entrance and stop-bar detectors for the three intersections for every signal cycle between 16:30:00 and18:30:00. Figure 6.3 and Figure 6.4 indicate that SPM generates consistent results with the ground truth. Table 6.1 also shows the mean percentage error (MPE) and mean absolute percentage error (MAPE) (Eq.(19)). The MAPEs are relative large (>10%). One reason is that we compared the throughput for each cycle (3 mins cycle length). When we aggregated data into 15min (5 cycles), the MAPEs for entrance and stop-bar detectors are decreased to 7.8% and 8.7% respectively. The other reason could be that we assume the same saturation flow rate, free flow speed, and jam density for all three intersections. If we calibrate these parameters, the results could be more accurate. But overall, these results validate that SPM can accurately describe traffic flow propagation.

$$\begin{cases} MPE = \dfrac{1}{m}\sum_{m}\left(\dfrac{Observation - Estimation}{Observation}\right)\times 100\% \\ MAPE = \dfrac{1}{m}\sum_{m}\left|\dfrac{Observation - Estimation}{Observation}\right|\times 100\% \end{cases} \tag{19}$$

where m is the sample size.

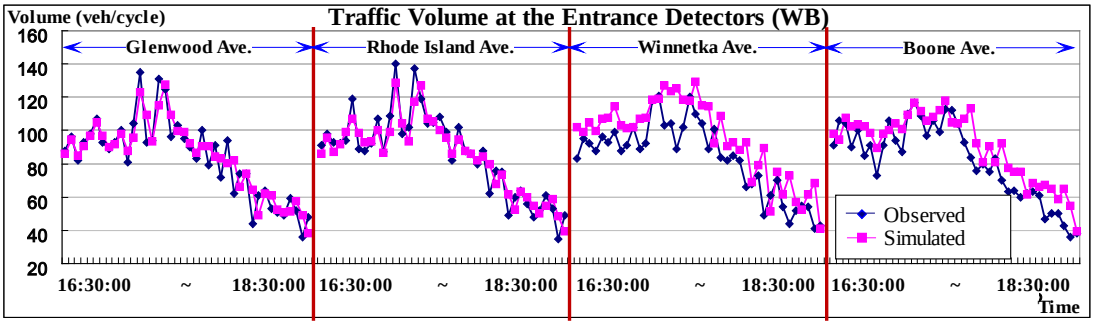

Figure 6.3 Comparison of Observed and Simulated Traffic Volumes for Four Entrance Detectors

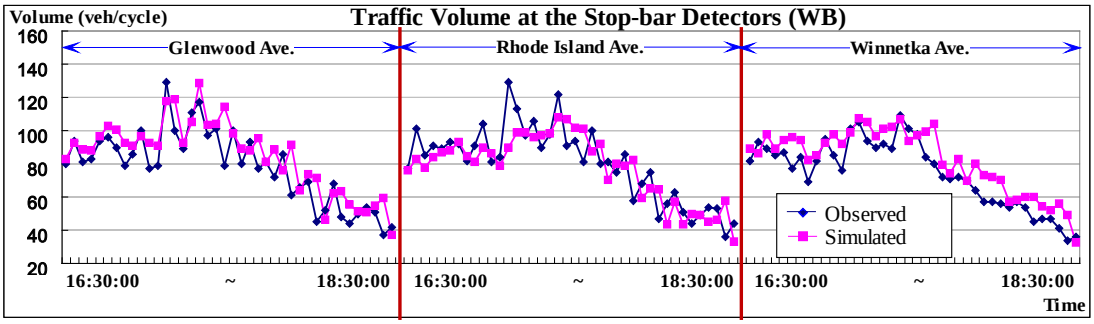

Figure 6.4 Comparison of Observed and Simulated Traffic Volumes for Three Stop-bar Detectors

Table 6.1 Comparison of Error Rates of Traffic Volumes from Two Types of Detectors

	MPE	MAPE
Entrance Detectors	**5.51%**	**12.3%**
Stop-bar Detectors	**4.25%**	**13.8%**

This experiment also demonstrates that SPM can accurately simulate traffic dynamics with spillovers. Figure 6.5 presents the shockwave dynamics from 17:05:00 to 17:42:00 on the two westbound links between Glenwood Ave. and Winnetka Ave. In SPM, the two links are represented by nodes 15, 17, 18, and 20 (see Figure 6.2). As mentioned before, during this time period, queue spilled back from the intersection of Winnetka Ave., creating spillover for the intersection at Rhode Island Ave. The spillover is successfully captured by SPM. As indicated in

Figure 6.5, SPM creates small new red phases (marked as the pink dash bars in the figure) within these spillover cycles. Figure 6.6 compares the time duration of the spillovers. The results indicate that SPM estimates a longer oversaturation period as spillover starts one cycle early and ends one cycle late. The reason could be the numerical errors generated at some time instants. For example, vehicles cannot be transferred from one section to another if the free-flow traveling distance within a time interval is longer than the distance between the tail end of the downstream queue and the section entrance. But in reality, vehicles can move slower (less than free-flow speed) and join the downstream queue. So SPM requires a little bit longer time to discharge queues at the upstream, particularly when the downstream section is congested.

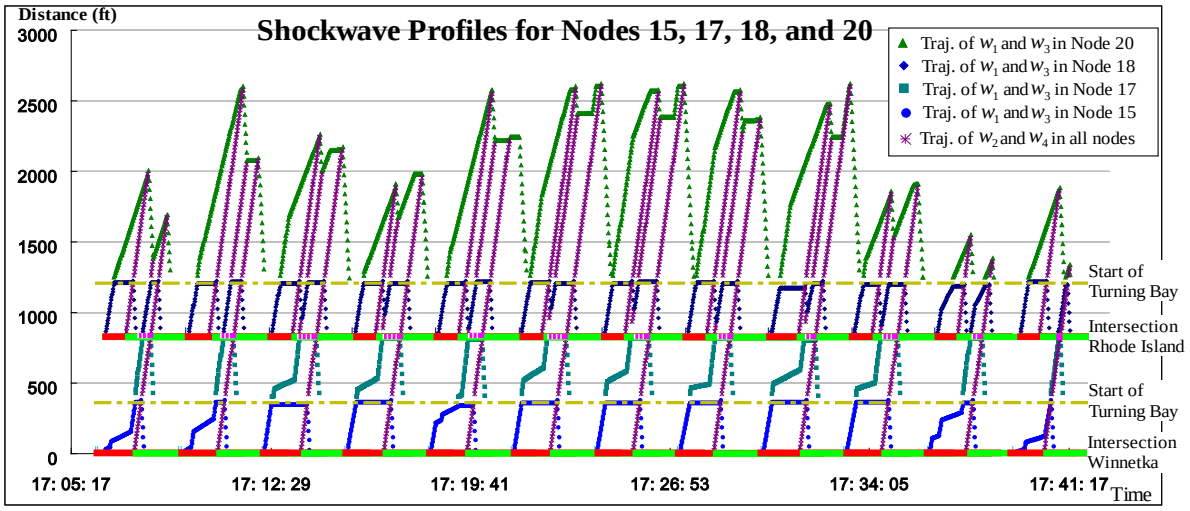

Figure 6.5 Shockwave Profiles for Nodes 15, 17, 18 and 20

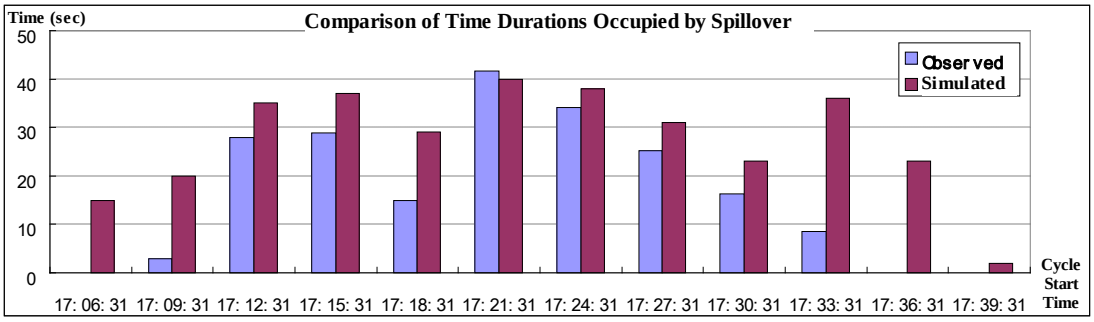

Figure 6.6 Comparison of Time Lengths Occupied by Spillovers

Chapter 7. Concluding Remarks

Arterial travel time and delay are important performance measures for both road travelers and traffic engineers. To estimate arterial travel time and delay, the key element is to estimate intersection queue length, since travel time, delay, and level of services can be easily derived from queue length information. In this report, we extend the virtual probe model to estimate arterial travel time with congested links. Specifically, we introduce into the virtual probe model a new queue length estimation approach, named SPM.

The proposed simplified SPM simulates the traffic dynamics on a congested urban network. Taking advantage of the fact that traffic states within a congested link can be simplified as free-flow, saturated, and jammed conditions, the SPM simulates the traffic dynamics by deriving the trajectories of shockwaves analytically. Each link with the same number of lanes is treated as a section in this model. The queuing dynamics within each section are described by tracing the shockwave fronts which explicitly separate the three traffic states. The SPM is specifically designed to deal with saturated or oversaturated arterials. In this model, a novel design is developed to treat spillover as either extending a red phase or creating new smaller cycles. This model is promising for analytical investigations of traffic in congested signalized arterials especially with queue spillovers. Therefore, the SPM is highly appropriate for large network real-time applications, especially when traffic is oversaturated. Using the "event" data (including both time-stamped signal phase changes and vehicle-detector actuations) collected from traffic signal systems, time-dependent queue length can be derived by examining the changes in signal detector's occupancy profile within a cycle. A field study at Trunk Highway 55 in the Twin Cities shows promising results.

For future research, we expect that the SPM can be further applied in traffic signal optimization. As a traffic flow model, the SPM provides a way to bridge the relationship between signal timing and intersection performance, so that a signal optimization program can be formulated by maximizing benefits (travel time savings, intersection throughput, etc.) or minimizing costs (queue, travel time, delay, etc.).

References

B&B Electronics. (2007). *Model 485SD9TB Port-Powered RS-485 Converter*. Retrieved March 30, 2007, from B&B Electronics: http://www.bb-elec.com/bb-elec/literature/485sd9tb-3803ds.pdf.

Cheu, R.L., Lee, D-H, and Xie, C. (2001). "An arterial speed estimation model fusing data from stationary and mobile sensors", *Proceedings of the IEEE Intelligent Transportation Systems Conference*, Oakland, CA, 573-578

Daganzo, C. (1994). "The cell transmission model: A dynamic representation of highway traffic consistent with the hydrodynamic theory", *Transportation Research Part B*, 28(4), 269-287.

Daganzo, C. (1995). "The cell transmission model: Part II: Network traffic", *Transportation Research Part B*, 29(2), 79-93.

Dell'Olmo, P. and Mirchandani, P. (1996). "A model for real-time traffic coordination using simulation based optimization", In Bianco and Toth (Eds.), *Advanced Methods in Transportation Analysis*. Springer, Germany, 525-546.

Frechette, L. A. and Khan, A. M., (1998). "Bayesian regression-based urban traffic models", *Transportation Research Record*, 1644, 157-165.

Greenshields, B. D. (1935). "A study of traffic capacity", *Highway Research Board Proceedings*, 14, 448-477.

Hall, F.L., Allen, B.L., and Gunter, M.A. (1986). "Empirical analysis of freeway flow-density relationships", *Transportation Research Part A*, 20, 197-210.

Helbing, D. (2003). "A section-based queuing-theoretical traffic model for congestion and travel time analysis in networks", *Journal of Physics A*, 36, 593-598.

Koshi, M., Iwasaki, M., and Okhura, I. (1983). "Some findings and an overview on vehicular flow characteristics", In: *Proceedings of the 8th International Symposium of Transportation and Traffic Theory*, Toronto, Canada, 403–426.

Lighthill, M.J. and Whitham, G.B. (1955). "On kinematic waves I Flood movement in long rivers. II A theory of traffic flow on long crowded roads", *Proceedings of the Royal Society A*, 229, 281–345.

Liu, H. and Ma, W. (2009). "A virtual vehicle probe model for time-dependent travel time estimation on signalized arterials", *Transportation Research Part C*, 17(1), 11-26.

Liu, H., Ma, W., Hu, H., Wu, X., and Yu, G. (2008). "SMART-SIGNAL: Systematic Monitoring of Arterial Road Traffic Signals", Presented at *11th International IEEE Conference on Intelligent Transportation System (ITSC)*, Beijing, China.

Liu, H., Ma, W., Wu, X., and Hu, H. (2010). "Real-Time Estimation of Arterial Travel Time under Congested Conditions", *Transportmetrica*, 8(2), 87-104.

Liu, H., Wu, X., Ma, W., and Hu, H. (2009). "Real-time queue length estimation for congested signalized intersections", *Transportation Research Part C*, 17(4), 412-427.

Michalopoulos, P. G., Stephanopoulos, G., and Pisharody, V. B. (1980). "Modelling of traffic flow at signalized links", *Transportation Sci*ence, 14(1), 9-41.

Michalopoulos, P. G., Beskos, D.E., and Lin, J.K. (1984). "Analysis of interrupted traffic flow by finite-difference methods", *Transportation Research Part B*, 18 (4-5), 409–421.

National Instruments. (2006). *NI-6528 User Guide and Specifications*. Retrieved January 30, 2007, from National Instruments: http://www.ni.com/pdf/manuals/372124a.pdf.

Papageorgiou, M. (1998). "Some remarks on macroscopic traffic flow modeling", *Transportation Research Part A*, 32(5), 323-329

Richards, P. J. (1956). "Shock waves on the highway", *Operations Research* 4, 42–51.

Takaba, S., Morita, T., Hada, T., Usami, T. and Yamaguchi, M., (1991). "Estimation and measurement of travel time by vehicle detectors and license plate readers", *Proceedings of Vehicle Navigation and Information Systems Conference*, 1, 257-267.

Turner, S., Lomax, T. J., and Levinson, H. S. (1996). "Measuring and Estimating Congestion using Travel Time-based Procedures", *Transportation Research Record*, 1564, 11-19.

Wu, X., Liu, H., and Gettman, D. (2010a). "Identification of Oversaturated Intersections Using High-Resolution Traffic Signal Data", *Transportation Research Part C*, 18(4), 626-638.

Wu, X., Liu, H., and Geroliminis, N. (2010b). "An Empirical Analysis on the Arterial Fundamental Diagram", *Transportation Research Part B*, 45 (1), 255-266.

Zhang, M. H. (1999). "Link-journey-speed model for arterial traffic", *Transportation Research Record*, 1676, 109-115.

Zhang, H.M. (2001). "Chapter 5: Continuum Flow Models", In: R. Kuhne and P. Michalopoulos (Eds.), *Traffic Flow Theory, A State-of-the-Art Report*, Transportation Research Board.